Fluid-Phase Chain Unsaturation Controlling Domain Microstructure and Phase in Ternary Lipid Bilayers Containing GalCer and Cholesterol

Wan-Chen Lin,* Craig D. Blanchette,*† and Marjorie L. Longo‡

*Biophysics Graduate Group, University of California, Davis, California; †Biophysical and Interfacial Science Group, Chemistry and Material Science, Lawrence Livermore National Laboratory, Livermore, California; and ‡Department of Chemical Engineering and Materials Science, University of California, Davis, California

ABSTRACT We report the microstructure and phase behavior of three ternary mixtures each containing a long-chain saturated glycosphingolipid, galactosylceramide (GalCer), and cholesterol at room temperature. The unsaturation level of the fluid-phase component was varied by lipid choice, i.e., saturated 1,2-dilauroyl-*sn*-glycero-3-phosphocholine (DLPC), singly unsaturated 1-palmitoyl-2-oleoyl-*sn*-glycero-3-phosphocholine (POPC), or doubly unsaturated 1,2-dioleoyl-*sn*-glycero-3-phosphocholine (DOPC). GalCer was used because of its biological significance, for example, as a ligand in the sexual transmission of HIV and stimulator of natural killer T-cells. Supported lipid bilayers of the ternary mixtures were imaged by atomic force microscopy and GalCer-rich domains were characterized by area/perimeter ratios (A/P). GalCer domain phase transitions from solid (S) to liquid (L) phase were verified by domain behavior in giant unilamellar vesicles, which displayed two-dimensional microstructure similar to that of supported lipid bilayers. As cholesterol concentration was increased, we observed ~2.5, ~10, and ~20-fold decreases in GalCer domain A/P for bilayers in L-S phase coexistence containing DOPC, POPC, and DLPC, respectively. The transition to L-L phase coexistence occurred at ~10 mol % cholesterol for bilayers containing DOPC or POPC and was accompanied by maintenance of a constant A/P. L-L phase coexistence did not occur for bilayers containing DLPC. We systematically relate our results to the impact of chain unsaturation on the interaction of the fluid-phase lipid and cholesterol. Physiologically, these observations may give insight into the interplay of fatty acid chain unsaturation, sterol concentration, and lipid hydrophobic mismatch in membrane phenomena.

INTRODUCTION

Glycosphingolipids isolated from plasma membranes are generally detergent-insoluble and are hypothesized to exist in ''rafts'' or lipid domains in the plasma membrane (1). This detergent-insoluble portion contains a high concentration of cholesterol (chol), which disrupts the acyl chain packing of long-chain saturated lipids and broadens the phase transition (2,3). As a result of this phenomenon, rafts are believed to exist in a liquid-ordered (L_o) phase (4,5) in which the lipids have high lateral mobility as in the fluid (L_α) phase, but their acyl chains are extended and ordered as in the solid (S) phase (6).

A glycosphingolipid of particular interest and biological relevance is galactosylceramide (GalCer). GalCer has been shown to act as an alternative receptor in the sexual transmission of HIV. In this pathway, an HIV envelope protein, gp120, binds to GalCer, initiating viral entry into colonic and vaginal epithelia cells, which lack the primary receptor CD4 (7–9). GalCer also plays an important role in natural killer T-cell activation (10–12), which is implicated in many immunological events that have important roles in health and disease (13–15). Because GalCer has been isolated from detergent-resistant membranes, it is believed to exist in phase-separated domains, and more likely in L_o domains, in cell membranes (1,16). However, very little work has been done using advanced techniques to study the microstructure and phase behavior of GalCer-rich domains, particularly in mixtures containing chol.

Our laboratory previously investigated phase separation and domain microstructures of 1,2-dilauroyl-*sn*-glycero-3-phosphocholine (DLPC)/GalCer/chol mixtures in bilayers at various chol concentrations (17). We found that this ternary lipid mixture only displays liquid (L)-S phase coexistence, and not L-L phase coexistence even at high chol concentrations (~20 mol %). Similar observations were reported in DLPC/1,2-dipalmitoyl-*sn*-glycero-3-phosphocholine (DPPC)/chol bilayers (18,19), whereas L-L coexistence was observed in 1,2-dioleoyl-*sn*-glycero-3-phosphocholine (DOPC)/DPPC/chol bilayers (20). Since DLPC is a saturated lipid and DOPC is a doubly unsaturated lipid, it appears that the unsaturation level of the fluid-phase component (the component which, in its pure hydrated form, is in the L_α phase at the observation temperature) in the ternary mixtures has a strong influence on the overall phase behavior. Physiologically, these observations may give insight into the role of fatty acid chain unsaturation in the plasma membrane (21,22).

It should be noted that L and S distinguish between distinct mechanical behaviors of bilayers; an S-phase bilayer behaves as a two-dimensional solid and an L-phase bilayer behaves as a two-dimensional fluid. S-phase lipid bilayers are typically in the L_B or L_B' phase. For pure lipid species in an S phase, the addition of chol typically results in the

Submitted August 18, 2006, and accepted for publication December 28, 2006.

Address reprint requests to Marjorie L. Longo, Dept. of Chemical Engineering and Materials Science, University of California, Davis, CA 95616. Tel.: 530-754-6348; Fax: 530-752-1031; E-mail: mllongo@ucdavis.edu.

0006-3495/07/04/2831/11 $2.00

doi: 10.1529/biophysj.106.095422

formation of some L_o phase within the L_B or L'_B phase at ~10 mol % chol (6,23,24). This fluidizes the bilayer, converting it to an L phase (25,26). As more chol is added, the L-phase bilayer continues to gain more L_o phase until it is completely L_o phase at ~25 mol % chol. It will continue to take on chol, remaining in L phase through the chol saturation level. Single-component L_α phase bilayers also exist in an L phase. The addition of chol may or may not result in the formation of some L_o phase, as will be discussed further below. Either way, as chol continues to be added, the bilayer remains in an L phase through the saturation level.

With respect to the saturation state of the fluid-phase component, chol exhibits stronger interaction with saturated PCs in comparison to unsaturated PCs. More specifically, both Lange et al. and Lund-Katz et al. showed that chol partitions with greater affinity into vesicles made of saturated phosphatidylcholine, PC (Di14PC or Di16PC) than into vesicles made of unsaturated PC (egg PC or DOPC) (27,28). In addition, using lipid monolayers, Smaby et al. showed that chol induced decreases in the monolayer elasticity and the magnitude of this decrease depended strongly on the structures of the acyl chains. Their study suggested that chol interacts with different PCs with affinity varying in the order Di14PC > 1-palmitoyl-2-oleoyl-*sn*-glycero-3-phosphocholine (POPC) > DOPC, in which the effect of chol on Di14PC monolayer can be several-fold larger than that on POPC and DOPC monolayers (29). Both electron spin resonance and differential scanning calorimetry studies showed that chol interacts with saturated PCs of various chain lengths strongly and in a similar way, whereas the interaction between chol and DOPC is different and much weaker (30–32). Moreover, reports that studied the phase behavior of binary mixtures composed of saturated PC and chol suggest that the L_o-phase lipid appears at low chol concentration, i.e., <8 mol % chol (24,33). As a comparison, its appearance in POPC/chol mixtures occurs at ~12 mol % chol (34), whereas it is absent for DOPC/chol mixtures (35). It should be noted that in the case of fluid-phase components, L_o-phase lipid occurs through cholesterol-induced chain extension, whereas the general property of lateral fluidity is retained.

In this report, we study the microstructure and phase behavior (e.g., L-L versus L-S) of three ternary mixtures DLPC/GalCer/chol, POPC/GalCer/chol, and DOPC/GalCer/chol over a range of chol concentrations. Based upon the discussion above, among the three fluid lipids that we used, chol interacts most strongly with DLPC and then POPC. As for DOPC, the interaction with chol is so weak that it is very unlikely that L_o-phase lipid would exist even at high chol concentration (34). Thus we can systematically relate GalCer domain microstructure and phase to the level of interaction between chol and the fluid-phase lipid.

Supported lipid bilayers (SLBs) of the three ternary mixtures were imaged by atomic force microscopy (AFM), providing detailed microstructural information regarding GalCer domains, e.g., area/perimeter ratios (A/P). We show that the unsaturation level of the fluid-phase component is critical to controlling chol-induced changes in GalCer domain microstructure, characterized by A/P. We show that A/P can represent domain interfacial line tension (γ) and we relate variations in the observed lowering in γ by chol to the ability of cholesterol to extend the chains of the various fluid-phase lipids. In general, we show that A/P tracks well with hydrophobic mismatch between the GalCer domains and the surrounding fluid-phase lipid. We compare domain microstructure of SLBs to giant unilamellar vesicles (GUVs) made from the same lipid mixtures and show that through our method of SLB preparation, two-dimensional microstructure in these systems is very similar. Domain phase transitions from S to L phase are verified by the domain behavior in the GUVs. We show that the unsaturation level of the fluid-phase component is critical to controlling chol-induced changes in phase of the GalCer domains. We relate these observations to variations in the phase partitioning of chol in the context of differences in interactions of cholesterol with fluid-phase lipids of different unsaturation levels. Our results give new insight into the complex phase behavior of lipid mixtures containing chol and can be applied to understand the phase behavior of more complicated system such as cell membranes.

MATERIALS AND METHODS

Materials

GalCer (bovine cerebrosides, a mixture of nonhydroxylated and hydroxylated GalCer, 75% saturated and 25% singly unsaturated, with tail lengths varying from 18 to 27 carbons (see 2005/2006 Matreya handbook, p. 92, Cat #1050, for exact percentage of each tail length)) was purchased from Matreya (Pleasant Gap, PA). DLPC, POPC, DOPC, cholesterol, and 1-palmitoyl-2-[6-[(7-nitro-2-1,3-benzoxadiazol-4-yl)amino]hexanoyl]-*sn*-glycero-3-phosphocholine (NBD-PC) were purchased from Avanti Lipids (Alabaster, AL). Glucose and sucrose were purchased from Sigma Chemicals (St. Louis, MO). All materials were used without further purification. All water used in these experiments was purified in a Barnstead Nanopure System (Branstead Thermolyne, Dubuque, IA) with a resistivity ≥17.9 MΩ and pH 5.5.

SLB preparation

Lipid mixtures in chloroform were dried in a clean glass reaction vial under a slow stream of N_2. The dried lipid film was resuspended with Nanopure water to a final lipid concentration of 0.1 mg/ml. The lipid suspension was incubated in a 70°C water bath for 5 min followed by a 15-s vortexing period. The lipid suspension, consisting of giant multilamellar vesicle (GMVs), was transferred to a plastic tube at room temperature before further treatment. A suspension of small unilameller vesicles (SUVs) was formed by sonicating the GMV suspension with a tip sonicator (Branson sonifier 250, Branson Ultrasonics, Danbury, CT) at the highest power until the suspension reached clarity. The suspension of SUVs was then incubated at room temperature to cool down for 10 min before further use. A 150-μl aliquot of the SUV suspension was deposited onto freshly cleaved room-temperature mica glued to a small metal puck. The vesicle droplet was allowed to incubate on the mica disk for 30 min and then rinsed 40 times with 80-μl

aliquots of purified water to remove excess vesicles. The sample was then dropped into a petri dish containing water and then placed into a preheated (50°C) temperature-controlled incubator (IN35, Torrey Pines Scientific, San Marcos, CA). After 1-h incubation at 50°C, the sample was cooled down slowly to room temperature in the oven at 10°C/h cooling rate.

AFM imaging

Samples were imaged with either a Digital Instruments (Santa Barbara, CA) NanoScope IIIa with a J scanner or Veeco Dimension 3100 Scanning Probe Microscope with Hybrid XYZ scanner (Santa Barbara, CA) in contact mode. Sharpened, coated AFM microlevers (Model MSCT-AUHW, Veeco) with nominal spring constants between 0.01 and 0.05 N/m were used for all scans. Hydration of the samples during scanning was maintained using a fluid cell (MMTFC, Veeco) when the J scanner was used. When the Hybrid XYZ scanner was used, samples were placed in a petri dish containing Nanopure water. To minimize the force applied to the surface, the scanning set point was frequently decreased until the tip left the surface and subsequently slightly increased until it just regained contact. Usually, the set points ranged between 0.1 and 0.2 V, with scan rates typically between 1 and 4 Hz, which approximately applied 20–300 pN force on the samples. At each composition of interest, at least three SLBs were imaged and measured. For each SLB, at least three AFM scans were performed. Depending on the domain size (ranging from tens of micrometers to hundreds of nanometers), each AFM image may have contained a few to ~50 GalCer domains. Domain size, area, and perimeter were measured by a public-domain software package, ImageTool (University of Texas Health Center, San Antonio, TX), which can detect and measure physical parameters of the height images produced from the AFM software. Domain height (height difference between the GalCer domain and the surrounding fluid phase) was obtained from section analysis of individual domains by the AFM software. In each AFM image, at least half of the domains were randomly picked to perform section analysis.

GUV preparation

Giant unilamellar vesicles were prepared using the electroformation method. Lipid mixtures containing 1 mol % NBD-PC were combined at various mole ratios (depending on the vesicle composition needed for experimentation) and dissolved in chloroform such that the final total lipid concentration was 1 mg/ml. Using a glass syringe, 50 μl of the lipid solution was coated evenly onto two parallel platinum wires, separated by 3 mm. The wires were housed in an open rectangular center of a Teflon block. The solvent was evaporated under a slow flow of nitrogen gas. The remaining solvent was removed by placing the wires under vacuum for at least 2 h. The open center of the block was sealed into a chamber by two SurfaSil (Pierce Biotechnology, Rockford, IL) coated glass coverslips using vacuum grease. The chamber was filled with a 100-mM sucrose aqueous solution that had been preheated to ~80°C. The chamber was then submerged in a 400-ml preheated sucrose solution and placed in an oven preheated to 80°C. A series of sine waves (3 V peak to peak) were applied across the wires at 10 Hz for 30 min, 3 Hz for 15 min, 1 Hz for 7 min, and 0.5 Hz for 7 min, using a function generator (Tenma, Centerville, OH). After the electroformation was complete, the chamber was slowly (2 h) cooled to room temperature and then allowed to equilibrate for 1 h. The vesicles were then harvested in Eppendorf vials. A 100-μl GUV suspension was then placed in a small chamber containing 100 mM glucose solution. GUVs were imaged 30 min later, when the vesicles had collected at the bottom of the chamber. This method resulted in GUVs ranging in size from 10 to 60 μm in diameter. The GUVs were used the same day of their preparation. Fluorescent imaging was carried out with a Nikon Eclipse 400 fluorescence microscope (Nikon, Melville NY) equipped with a fluorescence filter cube (EF-4 FITC HYQ, Nikon) that matches the excitation and emission spectrum of NBD-PC. Images were captured with a high-resolution Orca digital camera (Hamamatsu, Japan).

RESULTS

SLBs

The primary intent of this work is to study the impact of chol and acyl chain unsaturation of the fluid-phase component on GalCer domain microstructure and phase. We chose to use SLBs as a model membrane system, because AFM can be applied to obtain high-resolution images of the domain perimeter and thus the domain area/perimeter ratio (A/P) can be accurately determined. We use a technique called ''slow cooled vesicle fusion'' to form the SLBs. All SLBs were formed from SUVs containing 65 mol % fluid-phase lipids (i.e., the combined mole fraction of GalCer and chol was maintained at 35 mol %). Thirty minutes after depositing room-temperature SUVs onto freshly cleaved mica and rinsing, the sample was incubated at 50°C for 1 h and then slowly cooled to room temperature at a cooling rate of 10°C/h. We have previously shown that slow cooling applied to DLPC/GalCer/chol SLBs gave domain sizes and shapes comparable to observations in GUVs (17). By AFM, GalCer-rich domains appear as distinct lighter regions of constant height above the surrounding L phase. All samples were observed at room temperature.

In bilayers containing a ternary mixture of DOPC/GalCer/chol (the top row of images in Fig. 1), we observed a chol-dependent decrease in GalCer domain size from ~200 μm^2 to ~20 μm^2, corresponding to an increase from 0 mol % to 10 mol % chol, as quantified in Fig. 2. At and above 10 mol % chol, the domains remained roughly the same size and shape up to the point of lipid miscibility. The mixture reached the miscibility point at ~25mol % chol, as evidenced by the completely homogeneous appearance of the SLB. It should be noted that in general, it is plausible that within the apparent miscibility regimes observed here there existed nanometer-scale L_o GalCer-rich domains that we were unable to visualize due to a lack of phase height differences in AFM or resolution of optical fluorescence microscopy. We have addressed this possibility in a previous publication (17).

In POPC/GalCer/chol SLBs (Fig. 1, *middle row*), we observed a smaller average domain size at 0 mol % chol compared to DOPC/GalCer/chol SLB at 0 mol % chol. In addition, the chol-dependent decrease in domain size was more dramatic in comparison to DOPC/GalCer/chol SLBs, as shown in Fig. 2. The average GalCer domain area decreased from ~70 μm^2 to ~0.03 μm^2, corresponding to 0 mol % increased to 3 mol % chol. At 3 mol % chol, the nanometer-scale domains resided together to form micron-scale aggregates (see Fig. 3 *b* for the AFM image in larger scanning size). We observed the coexistence of nanometer-scale domains and a network microstructure at 5 mol % chol. Interestingly, above 5 mol % chol, the size of the GalCer domains increased to the previous micrometer scale and adopted shapes and sizes very similar to those observed in DOPC/GalCer/chol SLBs containing the same amount of chol. We

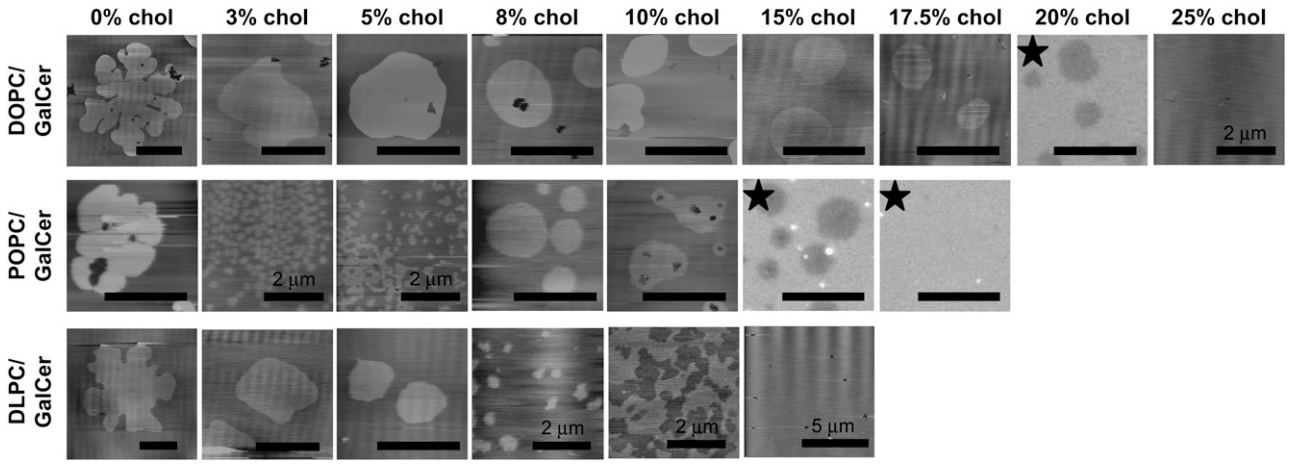

FIGURE 1 AFM height images and fluorescent images (labeled with a star) of supported lipid bilayers formed from DOPC/GalCer/chol (*top row*), POPC/GalCer/chol (*middle row*), and DLPC/GalCer/chol (*bottom row*) at various cholesterol concentrations. For SLBs containing 0 mol % chol, the mean values of domain height by section analysis were determined to be 0.85 ± 0.12 nm, 0.60 ± 0.07 nm, and 0.88 ± 0.11 nm for DOPC/GalCer, POPC/GalCer, and DLPC/GalCer SLBs, respectively. The mean height value of all other domains was <1 nm. Scale bars are 10 μm unless otherwise specified.

determined that lipid miscibility for the POPC/GalCer/chol mixture occurred at ~17.5 mol % chol.

It is worth noting that in both mixtures at ≥10 mol % chol, imaging domain microstructures in the SLBs with AFM became relatively difficult. The GalCer domains in these high-chol bilayers were much softer than those in low-chol bilayers and were easily pushed flat by the AFM tip, presumably due to fluidization of the domains. In addition, occasional regular vertical undulations were an artifact of the fast scanning rate that was necessary to image these softer bilayers. In the most extreme cases (DOPC/GalCer/20 mol % chol and POPC/GalCer/15 mol % chol), we were unable to obtain AFM images even using the softest AFM tips and lowest scanning forces available. Therefore, only fluorescent images (labeled by a star) are shown in Fig. 1 for these two mixtures. Since NBD-PC partitions weakly into GalCer, sphingomyelin, and long-chain saturated PC compared to the other lipid species used here (17,36,37), GalCer domains appear dark gray in the fluorescent images, whereas in the AFM images, domains are bright (which represents higher surface). In addition, GalCer domains in (DOPC or POPC)/GalCer/chol bilayers were often associated with defects that appear almost black in both AFM and fluorescent images. However, the defects did not appear to be impacting morphology, since defect-free domains of comparable appearance could always be found. In addition, the regions between the domains contained defects.

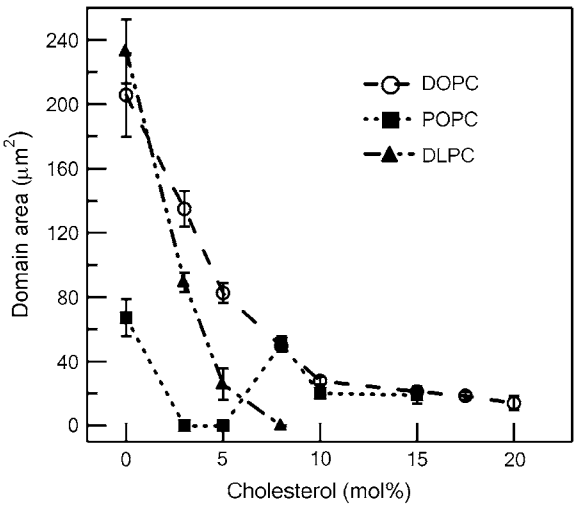

FIGURE 2 Average GalCer domain area as a function of cholesterol mole fraction. Bars indicate standard deviation.

For DLPC/GalCer/chol bilayers (Fig. 1, *bottom row*), we observed that GalCer domain size decreased from the micrometer scale to the nanometer scale (from ~200 μm^2 to ~0.10 μm^2) as chol was increased from 0 mol % to 8 mol %. A network microstructure was observed at 10 mol % chol. In contrast to POPC- and DOPC-containing ternary mixtures, micron-scale round domains were not observed at this chol concentration. The miscibility point was reached at ~15 mol % chol. The results for DLPC/GalCer/chol SLBs agree very well with our previous report on the phase behavior of the same mixture (17).

GUVs

We compared the domain microstructures of SLBs to GUVs, a model membrane system in which it is generally accepted that L- or S-phase domains approach their equilibrium size and shape. In these experiments, the lipid mixtures used to make GUVs were the same as those used to make SLBs. Fluorescence microscopy was used to observe microstructure and phase behavior of the GUVs. The GalCer domains

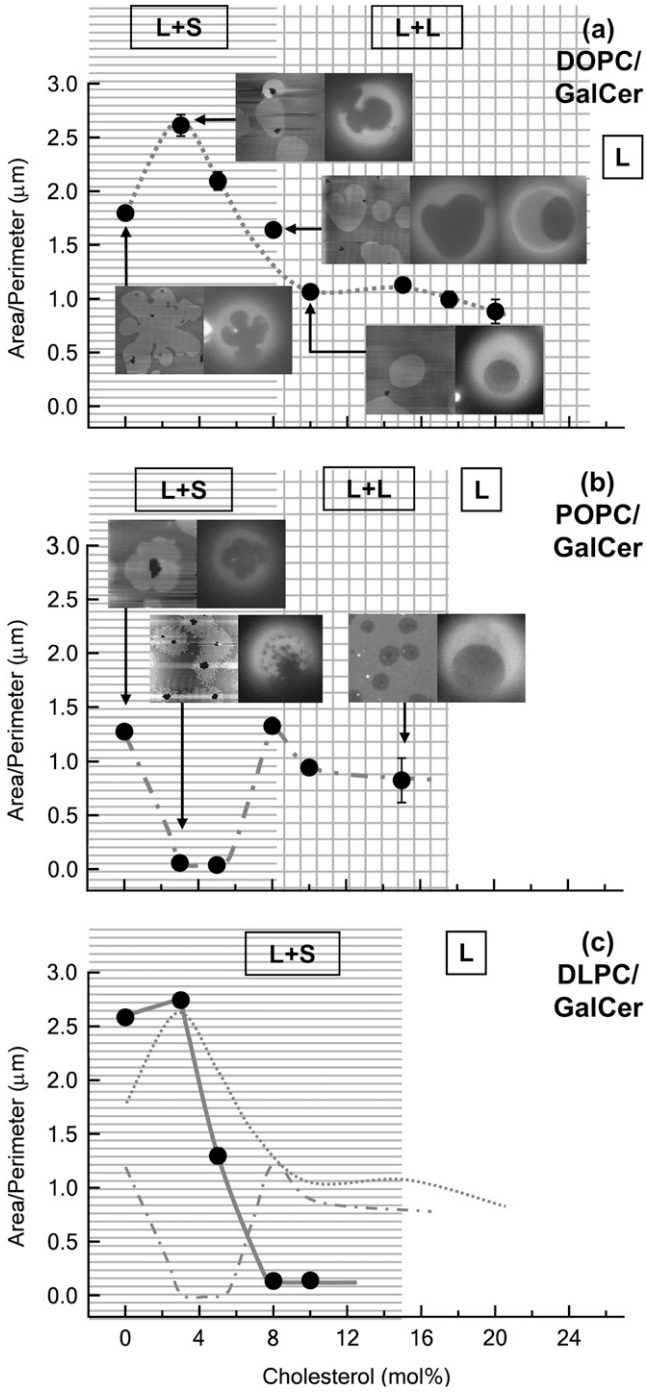

FIGURE 3 Area/perimeter ratio (A/P) as a function of cholesterol mole fraction and comparisons between SLBs and GUVs. At each point of interest (*arrows*), an AFM image of an SLB is presented next to a fluorescent image of a GUV that was made of the same lipid mixture. Each image is 20 μm $\times$ 20 μm. Phase labels: $L+S$, liquid-solid coexistence; $L+L$, liquid-liquid coexistence; L, one liquid phase. (*a*) DOPC/GalCer/chol mixture. Note that there are two GUV images shown for DOPC/GalCer/8 mol %-chol bilayer. (*b*) POPC/GalCer/chol mixture. (*c*) DLPC/GalCer/chol mixture (*solid line* and *data points*). For easy comparison between different mixtures, A/P curves of DOPC mixtures (*dotted line*) and POPC mixtures (*dash-dotted line*) are also presented.

appear dark, since NBD-PC was used as the fluorescence probe. At each chol concentration observed (Fig. 3, *solid circles*), we observed similarity in domain morphology and size comparing SLBs to GUVs. The key microstructures are demonstrated in Fig. 3, *a* and *b*, where at the chosen points, an AFM image of a SLB is presented next to one or two fluorescent images of a GUV that was made of the same lipid mixture. For all ternary mixtures as GUVs, when the chol content was $<$8 mol %, we observed typical L-S phase coexistence in which S domains rotated as rigid bodies, and did not coalesce with each other upon contact as described previously (20). S-phase domains do not merge due to the existence of repulsive interactions (20). Interestingly, at 3 mol % chol in POPC mixtures, the S domains on these GUVs displayed irregular shapes and blurry boundaries (Fig. 3 *b*). By comparing the domain microstructures observed in GUVs to SLBs (AFM images), we speculate that the domains on the GUV surface were actually composed of many smaller domains in close proximity, giving the appearance of a larger domain structure.

For (DOPC or POPC)/GalCer/chol at 8 mol % chol, we observed two populations of GUVs. Besides the ones that displayed L-S coexistence, we also found GUVs that exhibited L-L coexistence in which domains were circular with soft boundaries. When the chol concentration was 10 mol % and greater, L-L coexistence was the most prominent phase behavior observed. Therefore, we conclude with confidence that for (DOPC or POPC)/GalCer/chol SLBs and GUVs, the transition between L-S and L-L phase coexistence occurred between 8 mol % and 10 mol % chol (as noted on Fig. 3, *a* and *b*).

However, for DLPC/GalCer/chol at $\geq$8 mol %, the GalCer domains continued to behave as expected for the S phase. At 10 mol %, we observed a rigid network morphology. These results with respect to DLPC/GalCer/chol are in agreement with our previous work. L-S coexistence was always observed, even at compositions in which we were able to include 20 mol % chol (17). Therefore, we can confidently conclude that DLPC/GalCer/chol has a broad compositional region in which only L-S coexistence is exhibited. In addition, it is worth noting that the miscibility points in GUVs (images not shown) are the same as those in SLBs for all three mixtures, and these are noted in Fig. 3.

Area/perimeter ratio

We analyzed AFM images of our SLBs to obtain A/P by which we could relate our results to interfacial line tension (γ) at the GalCer domain boundaries. The measured A/P as a function of chol mole fraction for the three ternary mixtures is shown in Fig. 3. For DOPC/GalCer/chol mixtures (Fig. 3 *a*), we observed an initial $\sim$1.5-fold increase in A/P at 3 mol % chol followed by a chol-dependent decrease of $\sim$2.5-fold in A/P values from 3 mol % to 10 mol % chol. We attribute the initial increase to a transition in domain morphology

from leaflike (discussed later) to more round. When the chol content was ≥10 mol % (in which domains are in an L phase) the A/P value (~1 μm) did not change at increasing chol concentrations. For POPC/GalCer/chol bilayers (Fig. 3 *b*), we observed a 10-fold decrease in the A/P value when chol concentration was increased from 0% to 3 mol %. The A/P value remained the same when the chol concentration was further increased to 5 mol %. However, the A/P value increased 10-fold from 5 mol % to 8 mol % chol. Similar to the DOPC/GalCer/chol mixture, we also observed little change in A/P value at ≥10 mol % chol. In fact, at ≥8 mol % chol, the A/P values of POPC/GalCer/chol and DOPC/GalCer/chol bilayers were almost identical (see Fig. 3 *c* for comparison). For DLPC/GalCer/chol (Fig. 3 *c*), we observed a slight increase in A/P from 0 mol % chol to 3 mol % chol, which we attribute to rounding of the domains, as we did for the DOPC/GalCer/chol system. The A/P value then decreased by 20-fold as chol content increased from 3 mol % to 8 mol %. At 8 mol % and 10 mol % chol, we obtained the same low A/P value, ~0.1 μm. The results for DLPC agree very well with our previous report (17).

Domain height and fluorescence intensity

For SLBs containing 0 mol % chol, the mean values of domain heights by section analysis (i.e., height difference between domains, lighter regions in AFM images, and their surrounding) was determined to be 0.85 ± 0.12 nm, 0.60 ± 0.07 nm, and 0.88 ± 0.11 nm for DOPC/GalCer, POPC/GalCer, and DLPC/GalCer bilayers, respectively. The height difference between domains and the surrounding region in each mixture is consistent with S-phase GalCer domains contained in only one leaflet surrounded by fluid-phase lipid (Fig. 4, *a* and *b*). This interpretation is reached by comparison with diffraction measurements in which the steric bilayer thickness for bovine brain extract GalCer is 6.6 nm (38) and the steric bilayer thickness of the fluid-phase components used in this study are 4.4–4.5 nm for DOPC (39,40); 4.5 nm for POPC (40), and 3.9 nm for DLPC (41). Additionally, we performed fluorescence-intensity line scans for all fluorescent SLB images in which the domains were associated with large defects, extending to the mica. The defect allowed us to determine the level of background to subtract from the rest of the line scan. After subtracting background, we found that the fluorescence intensity in 71 GalCer domains was 47.3 ± 5.5% of the intensity of the surrounding fluid lipid region, as shown by the example in Fig. 5 *a* for a domain in a POPC/GalCer/8 mol % chol SLB. In agreement with the AFM section analysis, it is likely that the domain region comprised opposing leaflets of GalCer containing no fluorescent probe and fluid lipid containing fluorescent probe. Previously, we noted that the observed GalCer domain distributions for SLBs formed through vesicle fusion may be related to an asymmetric distribution of GalCer within the SUVs before supported lipid bilayer formation (17). Our results can also be used to gauge that the magnitude of the hydrophobic mismatch between GalCer and the surrounding region rich in fluid-phase lipid is as follows: DOPC ≈ DLPC > POPC (Fig. 6, *top row*). Interestingly, this order differs from the diffraction data quoted

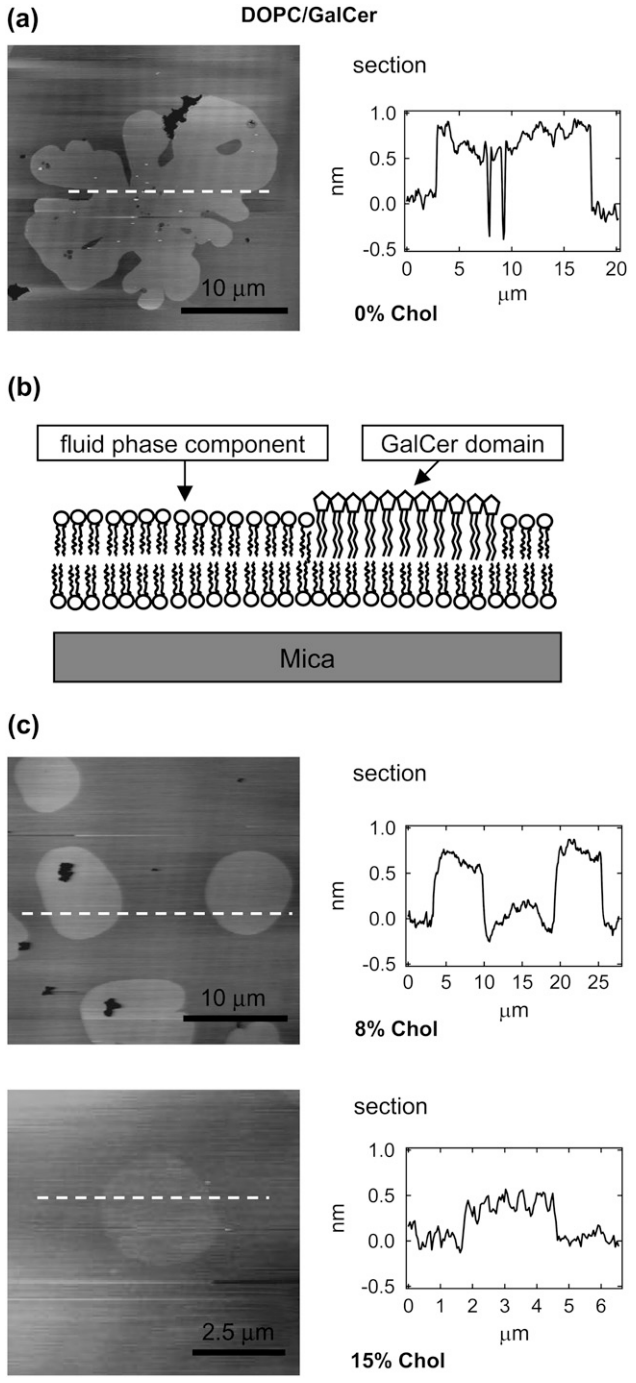

FIGURE 4 AFM height images and section analyses (*dashed lines* denote the location of the sections) of SLBs containing GalCer domain(s). (*a*) DOPC/GalCer. (*b*) An illustration showing that GalCer is distributed to the leaflet distal to the substrate. (*c*) DOPC/GalCer/8% mol % chol. and DOPC/GalCer/15% mol % chol.

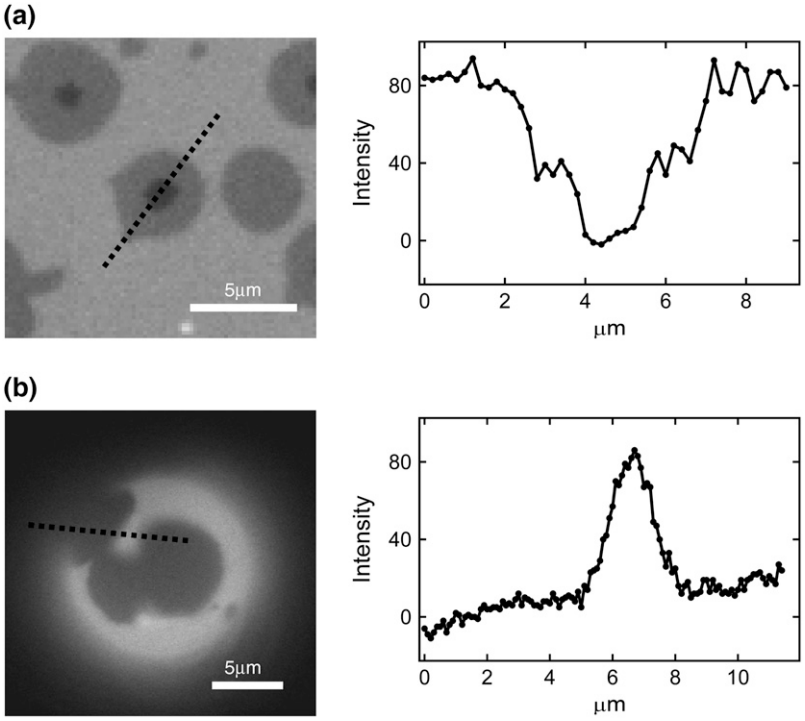

FIGURE 5 Fluorescence images and fluorescence pixel intensity line scans (*dashed lines* denote location of line scans) through (*a*) POPC/GalCer/8 mol % chol SLB containing domain with large defect, and (*b*) DOPC/GalCer/3 mol % chol GUV containing one domain in the middle of the field of view and another on the edge of the GUV. For the SLB, background intensity was set at the pixel intensity in the middle of the defect and subtracted out. For the GUV, background intensity was set at the pixel intensity of the line scan just outside the edge of the GUV and subtracted out.

above, which would put DOPC with POPC. In addition, as chol was added, mean domain heights remained at <1 nm, as illustrated by section analysis in Fig. 4 *c*. Although we believe it is unlikely, there may be possibilities other than lipid asymmetry for the height and fluorescence observations, including unusually high enrichment (>15 mol %) of the fluid lipid in the GalCer domains.

For comparison, we performed fluorescence-intensity line scans for all fluorescent GUV images in which a domain existed on the edge of the field of view of the GUV. For these domains, there is a minimum of background fluorescence from the rest of the GUV. We took background as the level of fluorescence intensity just outside (within 1 μm) of the domain on the edge of the GUV. After subtracting background

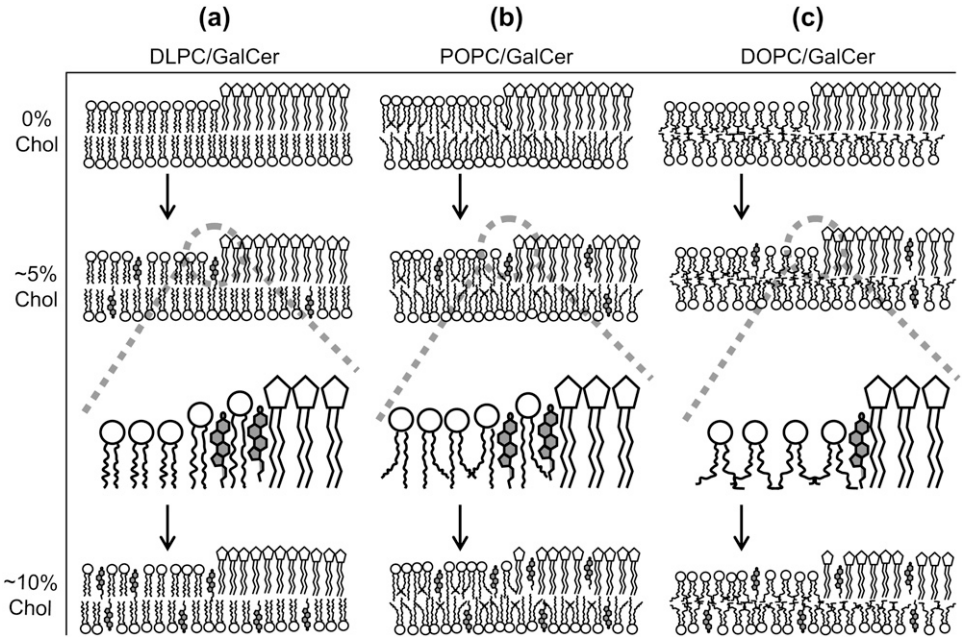

FIGURE 6 Proposed model of partition behavior of cholesterol and the effect of cholesterol at GalCer domain edges in (*a*) DLPC/GalCer/chol mixtures, (*b*) POPC/GalCer/chol mixtures, and (*c*) DOPC/GalCer/chol mixtures. In DLPC/GalCer/chol mixtures, cholesterol partitions in the fluid phase region only, whereas in POPC/ or DOPC/GalCer/chol mixtures, cholesterol partitions in both fluid regions and GalCer domains. The effect of cholesterol at the domain interface is depicted in the magnified part of the bilayers. Cholesterol may extend DLPC or POPC at the domain perimeter such that the domain line tension is lowered. Interaction between cholesterol and DOPC is so weak that this extension is unlikely to be pronounced enough to have an impact on domain line tension.

for domains in 81 GUVs, we found that the fluorescence intensity in the GalCer domains was 7.6 ± 13.3% of the intensity of the surrounding fluid lipid region, as shown by the example in Fig. 5 *b* for a domain in a DOPC/GalCer/3 mol % chol GUV. These results indicate that the GalCer domains in GUVs were symmetric; in other words, they comprised opposing leaflets of GalCer. This finding of domain symmetry is consistent with all other observations of lipid domains in GUVs, to the best of our knowledge.

DISCUSSION

Relating area/perimeter ratios to domain line tensions

Through careful control of thermal history during sample preparation, we demonstrate here and in another recent study (17) that domain microstructure in SLBs is reflective of two-dimensional domain microstructure in GUVs. AFM can be readily applied to SLBs containing coexisting phases to obtain detailed morphological information, such as A/P, not easily accessible in GUVs.

In general, A/P values can be considered an indicator of γ between the domain phase and the surrounding L phase. Fundamental thermodynamic principles give us an equation regarding self-assembled aggregates (GalCer domains in our case) and its monomer (GalCer solubilized in the L phase surrounding the domains) at equilibrium (see appendix for details).

$$-a_0\frac{P}{A}\gamma = CkT - \left(\mu^0_{\text{fluid}} - \mu^0_{\infty}\right),$$

where a_0 is the area/GalCer lipid, γ is the interfacial line tension at the domain perimeter, and μ^0_{fluid} and μ^0_{∞} are the standard chemical potentials of a GalCer molecule in the surrounding L region and in an infinite GalCer domain, respectively. The constant C varies with the solubility of GalCer in the surrounding L phase. For example, $C = 3.0$ and 2.3 when there is 5 mol % and 10 mol % GalCer, respectively, in the surrounding L phase. When two bilayers contain the same type of lipid mixtures (i.e., $\mu^0_{\text{fluid}} - \mu^0_{\infty}$ is about the same) and similar chol content (such that the solubility of GalCer in the surrounding L phase is similar), one can assume that the righthand side of the above equation is constant. Based on this assumption, γ should be proportional to the domain area/perimeter ratio, A/P. A nucleation and growth argument that does not assume equilibrium, discussed later, gives the same basic conclusions.

0% cholesterol

The origin of γ at the domain edge is believed to be the hydrophobic mismatch between the two phases. It has been reported extensively that lipids both stretch and deform at the domain interface to compensate for the hydrophobic mismatch and prevent hydrophobic exposure (42–44). Based on our domain height measurements, it appears that among the three different fluid lipids that we have investigated, POPC, with one 16:0 saturated and one 18:1 unsaturated acyl chain, has the smallest hydrophobic mismatch with GalCer domains, and DLPC and DOPC have a similar level of hydrophobic mismatch to GalCer domains (Fig. 6, *top row*). As a result, the POPC/GalCer SLB contained the smallest domains (with diameters <10 μm) and had an A/P value lower than observed in DOPC/GalCer and DLPC/GalCer bilayers.

In addition to γ, the dipole repulsion can have a large effect on S-phase domain shapes, especially when the domains are large (45). It has been shown that during 2-D domain growth in a monolayer, a domain starts to adopt a leaflike shape only when the domain reaches a certain size (46). Interestingly, we observed similar behavior in our SLBs regarding domain shapes; only those with diameters >15 μm adopted a leaflike shape. We speculate that the long-range electrostatic dipolar repulsions between S-phase lipids in the domains is the main reason for the leaflike shape, as this force is known to favor elongated domains (45). Leaf-shaped domains have larger domain perimeters compared to circular ones. This explains the lower A/P values of 0 mol % chol bilayers compared to 3 mol % chol bilayers in both DOPC/GalCer/chol and DLPC/GalCer/chol mixtures.

Less than 8 mol % cholesterol

In the case of DLPC/GalCer/chol, we previously related lowering of A/P to strong chol partitioning at the domain perimeter, resulting in extended DLPC chains and, thus, decreased hydrophobic mismatch with GalCer (Fig. 6 *a*) and lowered γ. As a result, we observed stable nanometer-scale S-phase domains and low A/P values for bilayers containing chol (17). Similarly, for the POPC/GalCer/chol mixture, the same mechanism can explain the formation of nanometer-scale S-phase domains at 3 mol % chol. With its one saturated acyl chain, POPC has the ability to interact with chol, hence lowering domain γ by extending the acyl chain (Fig. 6 *b*). Nezil and Bloom reported that the thickness of the POPC bilayer can increase by 0.4 nm upon addition of 30 mol % chol (47). According to a theoretical calculation by Kuzmin et al., a 0.2-nm decrease in hydrophobic mismatch in a monolayer can easily lead to a γ that is >10 times lower (44). Interestingly, the A/P values (an indicator of γ) in the POPC/GalCer supported bilayers containing 0 mol % and 3 mol % chol are $\sim$1.0 μm and $\sim$0.1 μm, respectively. It is worth noting that in our POPC/GalCer/3 mol % chol SLB, only 0.02 mol % chol is needed to saturate the entire domain perimeter under the assumptions that the ''perimeter region'' contains three layers of lipids and chol reaches saturation at 40 mol %. Thus, the domain perimeter can be easily saturated at 3 mol % chol. This may explain why we did not observe a further decrease in size and A/P value when chol concentration was increased from 3 mol % to 5 mol %. The hydrophobic mismatch between the

GalCer domain and surrounding POPC is much smaller than that between GalCer and DLPC. Thus, we observed a drop in A/P at lower chol concentration for POPC mixtures compared to DLPC mixtures.

On the contrary, for the DOPC/GalCer/chol mixtures, due to the weak interaction between DOPC and chol, we did not observe a significant decrease of A/P during L-S phase coexistence. Chol may simply serve as an impurity at the interface (Fig. 6 *c*) whereby the γ decreases slowly, as does A/P, as chol concentration increases. Another possibility is that chol at the GalCer domain perimeter decreases the elastic modulus of the GalCer perimeter (26), thus gently lowering γ. Through theoretical calculation, the effect of mechanical properties on γ is not as significant as that of hydrophobic mismatch (44).

Greater than 8 mol % cholesterol

As illustrated in Fig. 6, our results indicate that chol exhibits different phase-partition behavior in DLPC/GalCer/chol bilayers versus (POPC or DOPC)/GalCer/chol bilayers, although we observed similar phase behavior between DLPC mixtures and POPC mixtures at low chol concentrations. Due to its strong interaction with DLPC, chol partitions strongly with DLPC even at high chol concentrations, i.e., $\geq$10 mol %. In other words, GalCer domains are always in the S phase in DLPC/GalCer/chol mixtures. On the other hand, for (DOPC or POPC)/GalCer/chol bilayers, chol is present in both the GalCer domains and the surrounding phase, as evidenced by the formation of L-phase GalCer domains at higher chol concentrations. The transition to L-L phase coexistence occurs at $\sim$10 mol % chol, which is the typical chol mole fraction required for long-chain saturated lipid to become liquefied due to the initial appearance of the L_o phase (25,26). This agreement indicates that at 10 mol % chol, there is relatively even partitioning of chol between DOPC or POPC and GalCer in the bilayer. At higher chol concentration, there may be cooperative enrichment of chol into the GalCer domains. We speculate that the partition behavior of chol is very similar in DOPC/GalCer/chol and POPC/GalCer/chol mixtures, as evidenced by the same A/P at $\geq$8 mol % chol. This similar A/P also indicates that in L-L coexistence, the chol-GalCer interaction is the dominant factor in domain morphology (and thus determining A/P), whereas the fluid-phase lipid component has little effect.

Thermodynamic considerations

For carefully prepared samples, it is reasonable to treat the domain size distribution and domain shape in SLBs as thermodynamic phenomena, as in the case of GUVs, which results from the balance between entropy, line tension at domain perimeter, and long-range dipole-dipole repulsion. Compared to a GUV, an SLB can be considered a system that contains an infinite number of lipids. On the contrary, due to the limitation and variation of GUV sizes, it is difficult to compare domain size distribution from different lipid mixtures. In contrast to the GUV system, domains in SLBs are immobile. Nevertheless, domain merging is not a major mechanism for growth of domains in the S phase due to dipolar interactions. In the case of domains in the L phase, domain merging is a major mechanism of growth in GUVs. In SLBs, L-phase domain merging is only observed when domains grow into each other. However, we find that L-phase domains grow to similar size in GUVs and SLBs. This phenomenon probably results from the limited size of the GUVs, which limits domain merging to those present on the GUVs compared to the infinite pool of lipids available for domain growth in SLBs. SLBs and GUVs can vary in domain symmetry. An asymmetric domain should have half the γ of a symmetric domain, since there is half the hydrophobic mismatch with its fluid lipid neighbors. We expect that chol will have the same relative impact on γ for either type of domain, and thus the same trends in A/P ratio in both GUVs and SUVs. But the fact that the sizes of the domains can be made similar in this study indicates that factors such as the exact temperature of domain nucleation in these two systems and vesicle size are playing an important role. Overall, it is clear that ''equilibrium'' is not truly reached in either GUVs or SLBs. An alternative viewpoint involving nucleation and growth may be equally appropriate.

In addition to the equilibrium analysis presented earlier, a similar relationship between A/P and γ can be obtained through classical theory of nucleation. According to classical theory of nucleation, the nucleation rate depends on γ, where higher γ results in slower nucleation rates. Thus, high γ results in fewer nucleation events and lower γ results in more nucleation events. The size of domains in turn depends on the number of nucleation events that occur once the bilayer has been cooled below the miscibility point; if, e.g., the number of nucleation events is relatively low, then domain microstructures will be large. The A/P ratio depends strongly on domain size, with larger domains having much higher A/P ratios. Therefore, a high A/P reflects high γ and low A/P reflects low γ. This will be the subject of a subsequent article in which we measure lipid domain nucleation rates and explicitly calculate γ for symmetric and asymmetric domains in SLBs.

It is important that nucleation events not be ''seeded'' by defects present in the SLB. We believe that the defects observed here occurred after domain nucleation as a result of the overall area/molecule decreasing during the phase transition. This conclusion is reached because defect-free domains did not display different morphology in comparison to defect-containing domains. Additionally, defects were observed everywhere, not just within domains, although they more often were seen associated with domains.

CONCLUSION

In conclusion, we have compared the microstructure and phase behavior of three ternary mixtures, each containing

GalCer, chol, and a fluid-phase lipid component with a different unsaturation level. Thus we systematically varied the interaction between chol and the fluid-phase lipid (DLPC > POPC > DOPC). We found that the GalCer domain microstructure and phase were affected by the interaction strength between fluid-phase lipid and chol and also by related partition behavior of chol. Our findings point to a complex interplay between acyl chain unsaturation, hydrophobic mismatch, and sterol concentration controlling microstructure and dynamics in multi-component lipid systems such as cell membranes.

APPENDIX

Equilibrium thermodynamics requires that in a system of molecules that form aggregated structures (GalCer domains in our case) the chemical potential of identical molecules in different phases be the same. This may be expressed as

$$\mu^0_{\text{fluid}} + kT \ln \chi_{\text{fluid}} = \mu^0_{\text{domain}} + \frac{kT}{N} \ln\left(\frac{\chi_{\text{domain}}}{N}\right), \qquad (1)$$

where μ^0_{fluid} and $\mu^0_{\text{domain}} = \mu^0_\infty + P\gamma/N$ are the standard chemical potential of GalCer molecules in fluid region and domain, respectively. χ_{fluid} and χ_{domain} are the activity of GalCer in fluid region and domain, respectively. Typically, χ_{fluid}, also known as solubility of GalCer in the fluid phase, is ~0.1 and χ_{domain} is ~0.9 at low chol concentration. N is the number of GalCer molecules in a domain and is roughly equal to domain area A divided by area/GalCer lipid a_0. Equation 1 can be rearranged and modified with $\mu^0_{\text{domain}} = \mu^0_\infty + P\gamma/N$ where μ^0_∞ is the chemical potential of an infinite GalCer aggregate, P the perimeter of GalCer domain, and γ the interfacial line tension at domain perimeter (48). Equation 1 becomes

$$-a_0 \frac{P}{A} \gamma = kT \left[\ln \frac{\sqrt[N]{\chi_{\text{domain}}/N}}{\chi_{\text{fluid}}} \right] - \left(\mu^0_{\text{fluid}} - \mu^0_\infty\right). \qquad (2)$$

It can be shown that when N is large ($>10^4$), the right hand side of Eq. 2 is equal to $CkT - (\mu^0_{\text{fluid}} - \mu^0_\infty)$, where C varies only with χ_{fluid}, but not N and χ_{domain}. Since our smallest domain (~200 nm in diameter) contains $>7 \times 10^4$ GalCer lipids, it is fair to treat C as a constant when χ_{fluid} is a constant.

This work was performed under the auspices of the U.S. Dept. of Energy by the University of California/Lawrence Livermore National Laboratory under contract No. W-7405-Eng-48.

We acknowledge funding by the Nanoscale Interdisciplinary Research Teams Program of the National Science Foundation (under award Nos. CHE 0210807 and BES 0506602) and the Center on Polymer Interfaces and Macromolecular Assemblies (grant NSF DMR 0213618). C.D.B. acknowledges funding from grant T32-GM08799 from the National Institute of General Medical Sciences of the National Institutes of Health and the Student-Employee Graduate Research Fellowship (SEGRF) Program of Lawrence Livermore National Laboratory.

REFERENCES

1. Brown, D. A., and J. K. Rose. 1992. Sorting of Gpi-anchored proteins to glycolipid-enriched membrane subdomains during transport to the apical cell-surface. *Cell*. 68:533–544.
2. Ohvo-Rekila, H., B. Ramstedt, P. Leppimaki, and J. P. Slotte. 2002. Cholesterol interactions with phospholipids in membranes. *Prog. Lipid Res.* 41:66–97.
3. Ramstedt, B., and J. P. Slotte. 2002. Membrane properties of sphingomyelins. *FEBS Lett.* 531:33–37.
4. Silvius, J. R., D. Delgiudice, and M. Lafleur. 1996. Cholesterol at different bilayer concentrations can promote or antagonize lateral segregation of phospholipids of differing acyl chain length. *Biochemistry*. 35:15198–15208.
5. Brown, D. A., and E. London. 2000. Structure and function of sphingolipid- and cholesterol-rich membrane rafts. *J. Biol. Chem.* 275: 17221–17224.
6. Ipsen, J. H., G. Karlstrom, O. G. Mouritsen, H. Wennerstrom, and M. J. Zuckermann. 1987. Phase dquilibria in the phosphatidylcholine-cholesterol system. *Biochim. Biophys. Acta*. 905:162–172.
7. Bhat, S., S. L. Spitalnik, F. Gonzalez-Scarano, and D. H. Silberberg. 1991. Galactosyl ceramide or a derivative is an essential component of the neural receptor for human immunodeficiency virus type 1 envelope glycoprotein gp120. *Proc. Natl. Acad. Sci. USA*. 88:7131–7134.
8. Fantini, J., D. G. Cook, N. Nathanson, S. L. Spitalnik, and F. Gonzalezscarano. 1993. Infection of colonic epithelial-cell lines by type-1 human-immunodeficiency-virus is associated with cell-surface expression of galactosylceramide, a potential alternative Gp120 receptor. *Proc. Natl. Acad. Sci. USA*. 90:2700–2704.
9. Clapham, P. R., A. McKnight, S. Talbot, and D. Wilkinson. 1996. HIV entry into cells by CD4-independent mechanisms. *Perspect. Drug Discov. Des.* 5:83–92.
10. Taraschi, T. F., A. Wu, and E. Rubin. 1985. Phospholipid spin probes measure the effects of ethanol on the molecular order of liver-microsomes. *Biochemistry*. 24:7096–7101.
11. Kronenberg, M., and A. Rudensky. 2005. Regulation of immunity by self-reactive T cells. *Nature*. 435:598–604.
12. Meyer, E. H., S. Goya, O. Akbari, G. J. Berry, P. B. Savage, M. Kronenberg, T. Nakayama, R. H. DeKruyff, and D. T. Umetsu. 2006. Glycolipid activation of invariant T cell receptor(+) NK T cells is sufficient to induce airway hyperreactivity independent of conventional CD4(+) T cells. *Proc. Natl. Acad. Sci. USA*. 103:2782–2787.
13. Jerud, E. S., G. Bricard, and S. A. Porcelli. 2006. CD1d-restricted natural killer T cells: roles in tumor immunosurveillance and tolerance. *Transfus. Med. Hemother.* 33:18–36.
14. Parekh, V. V., M. T. Wilson, and L. Van Kaer. 2005. iNKT-cell responses to glycolipids. *Crit. Rev. Immunol.* 25:183–213.
15. Van Kaer, L. 2004. Natural killer T cells as targets for immunotherapy of autoimmune diseases. *Immunol. Cell Biol.* 82:315–322.
16. Thompson, T. E., and T. W. Tillack. 1985. Organization of glycosphingolipids in bilayers and plasma-membranes of mammalian-cells. *Annu. Rev. Biophys. Biophys. Chem.* 14:361–386.
17. Blanchette, C. D., W. C. Lin, T. V. Ratto, and M. L. Longo. 2006. Galactosylceramide domain microstructure: impact of cholesterol and nucleation/growth conditions. *Biophys. J.* 90:4466–4478.
18. Feigenson, G. W., and J. T. Buboltz. 2001. Ternary phase diagram of dipalmitoyl-PC/dilauroyl-PC/cholesterol: nanoscopic domain formation driven by cholesterol. *Biophys. J.* 80:2775–2788.
19. Korlach, J., P. Schwille, W. W. Webb, and G. W. Feigenson. 1999. Characterization of lipid bilayer phases by confocal microscopy and fluorescence correlation spectroscopy. *Proc. Natl. Acad. Sci. USA*. 96: 8461–8466.
20. Veatch, S. L., and S. L. Keller. 2002. Organization in lipid membranes containing cholesterol. *Phys. Rev. Lett.* 89:268101.
21. Mukherjee, S., T. T. Soe, and F. R. Maxfield. 1999. Endocytic sorting of lipid analogues differing solely in the chemistry of their hydrophobic tails. *J. Cell Biol.* 144:1271–1284.
22. Mukherjee, S., and F. R. Maxfield. 2004. Membrane domains. *Annu. Rev. Cell Dev. Biol.* 20:839–866.
23. Zhai, X., X.-M. Li, M. M. Momsen, H. L. Brockman, and R. E. Brown. 2006. Lactosylceramide: lateral interactions with cholesterol. *Biophys. J.* 91:2490–2500.
24. Mcmullen, T. P. W., and R. N. McElhaney. 1995. New aspects of the interaction of cholesterol with dipalmitoylphosphatidylcholine bilayers as revealed by high-sensitivity differential scanning calorimetry. *Biochim. Biophys. Acta*. 1234:90–98.

25. Needham, D., T. J. Mcintosh, and E. Evans. 1988. Thermomechanical and transition properties of dimyristoylphosphatidylcholine cholesterol bilayers. *Biochemistry*. 27:4668–4673.

26. Tierney, K. J., D. E. Block, and M. L. Longo. 2005. Elasticity and phase behavior of DPPC membrane modulated by cholesterol, ergosterol, and ethanol. *Biophys. J*. 89:2481–2493.

27. Lange, Y., J. S. Dalessandro, and D. M. Small. 1979. Affinity of cholesterol for phosphatidylcholine and sphingomyelin. *Biochim. Biophys. Acta*. 556:388–398.

28. Lundkatz, S., H. M. Laboda, L. R. Mclean, and M. C. Phillips. 1988. Influence of molecular packing and phospholipid type on rates of cholesterol exchange. *Biochemistry*. 27:3416–3423.

29. Smaby, J. M., M. M. Momsen, H. L. Brockman, and R. E. Brown. 1997. Phosphatidylcholine acyl unsaturation modulates the decrease in interfacial elasticity induced by cholesterol. *Biophys. J*. 73:1492–1505.

30. Pasenkiewiczgierula, M., W. K. Subczynski, and A. Kusumi. 1990. Rotational diffusion of a steroid molecule in phosphatidylcholine cholesterol membranes: fluid-phase microimmiscibility in unsaturated phosphatidylcholine cholesterol membranes. *Biochemistry*. 29:4059–4069.

31. Mcmullen, T. P. W., R. N. A. H. Lewis, and R. N. Mcelhaney. 1993. Differential scanning calorimetric study of the effect of cholesterol on the thermotropic phase-behavior of a homologous series of linear saturated phosphatidylcholines. *Biochemistry*. 32:516–522.

32. Davis, P. J., and K. M. W. Keough. 1983. Differential scanning calorimetric studies of aqueous dispersions of mixtures of cholesterol with some mixed-acid and single-acid phosphatidylcholines. *Biochemistry*. 22:6334–6340.

33. Vist, M. R., and J. H. Davis. 1990. Phase equilibria of cholesterol dipalmitoylphosphatidylcholine mixtures deuterium NMR and differential scanning calorimetry. *Biochemistry*. 29:451–464.

34. de Almeida, R. F. M., A. Fedorov, and M. Prieto. 2003. Sphingomyelin/phosphatidylcholine/cholesterol phase diagram: boundaries and composition of lipid rafts. *Biophys. J*. 85:2406–2416.

35. Lentz, B. R., Y. Barenholz, and T. E. Thompson. 1976. Fluorescence depolarization studies of phase-transitions and fluidity in phospholipid bilayers. 2. Two-component phosphatidylcholine liposomes. *Biochemistry*. 15:4529–4537.

36. Shaw, J. E., R. F. Epand, R. M. Epand, Z. Li, R. Bittman, and C. M. Yip. 2006. Correlated fluorescence-atomic force microscopy of membrane domains: structure of fluorescence probes determines lipid localization. *Biophys. J*. 90:2170–2178.

37. Wang, T.-Y., and J. R. Silvius. 2000. Different sphingolipids show differential partitioning into sphingolipid/cholesterol-rich domains in lipid bilayers. *Biophys. J*. 79:1478–1489.

38. Kulkarni, K., D. S. Snyder, and T. J. Mcintosh. 1999. Adhesion between cerebroside bilayers. *Biochemistry*. 38:15264–15271.

39. Wiener, M. C., and S. H. White. 1992. Structure of a fluid dioleoylphosphatidylcholine bilayer determined by joint refinement of x-ray and neutron-diffraction data. III. Complete structure. *Biophys. J*. 61: 434–447.

40. Kucerka, N., S. Tristram-Nagle, and J. F. Nagle. 2006. Structure of fully hydrated fluid phase lipid bilayers with monounsaturated chains. *J. Membr. Biol*. 208:193–202.

41. Kučerka, N., Y. Liu, N. Chu, H. I. Petrache, S. Tristram-Nagle, and J. F. Nagle. 2005. Structure of fully hydrated fluid phase DMPC and DLPC lipid bilayers using x-ray scattering from oriented multilamellar arrays and from unilamellar vesicles. *Biophys. J*. 88:2626–2637.

42. Trandum, C., P. Westh, K. Jorgensen, and O. G. Mouritsen. 2000. A thermodynamic study of the effects of cholesterol on the interaction between liposomes and ethanol. *Biophys. J*. 78:2486–2492.

43. Akimov, S. A., P. I. Kuzmin, J. Zimmerberg, F. S. Cohen, and Y. A. Chizmadzhev. 2004. An elastic theory for line tension at a boundary separating two lipid monolayer regions of different thickness. *J. Electroanal. Chem.* 564:13–18.

44. Kuzmin, P. I., S. A. Akimov, Y. A. Chizmadzhev, J. Zimmerberg, and F. S. Cohen. 2005. Line tension and interaction energies of membrane rafts calculated from lipid splay and tilt. *Biophys. J*. 88:1120–1133.

45. Mcconnell, H. M., and V. T. Moy. 1988. Shapes of finite two-dimensional lipid domains. *J. Phys. Chem.* 92:4520–4525.

46. Recktenwald, D. J., and H. M. Mcconnell. 1981. Phase-equilibria in binary-mixtures of phosphatidylcholine and cholesterol. *Biochemistry*. 20:4505–4510.

47. Nezil, F. A., and M. Bloom. 1992. Combined influence of cholesterol and synthetic amphiphillic peptides upon bilayer thickness in model membranes. *Biophys. J*. 61:1176–1183.

48. Israelachvili, J. 1992. Intermolecular and Surface Forces. Academic Press, San Diego.